MECHANICAL CHARACTERISATION OF ADDITIVELY MANUFACTURED ELASTOMERIC STRUCTURES FOR VARIABLE STRAIN RATE APPLICATIONS

Michael Robinson [a], Shwe Soe [a], Richard Johnston [b], Rhosslyn Adams [a], Benjamin Hanna [a], Roy Burek [a,c], Graham McShane [d], Rafael Celeghini [e], Marcilio Alves [f], Peter Theobald [a *]

[a] High Value Manufacturing Research Group, Cardiff School of Engineering, Cardiff University, Wales, United Kingdom.

[b] Advanced Imaging of Materials (AIM) Facility, College of Engineering, Swansea University, UK;

[c] Charles Owen, Royal Works, Croesfoel Industrial Park, Wrexham, UK.

[d] Department of Engineering, Trumpington Street, Cambridge University, UK.

[e] Centre of Engineering, Modelling and Applied Social Science (CECS), Federal University of ABC (UFABC), Brazil.

[f] Department of Mechatronics and Mechanical Systems Engineering. Group of Solid Mechanics and Structural Impact, University of São Paulo (USP), Brazil

*** Corresponding Author:** Dr P S Theobald, Cardiff School of Engineering, Cardiff University, The Parade, Cardiff, CF24 3AA, UK.

Abstract

Additive manufacturing (AM) enables production of geometrically-complex elastomeric structures. The elastic recovery and strain-rate dependence of these materials means they are ideal for use in dynamic, repetitive mechanical loading. Their process-dependence, and the frequent emergence of new AM elastomers, commonly necessitates full material characterisation; however, accessing specialised equipment means this is often a time-consuming and expensive process. This work presents an innovative equi-biaxial rig that enables full characterisation via just a conventional material testing machine (supplementing uni-axial tension and planar tension tests). Combined with stress relaxation data, this provides a novel route for hyperelastic material modelling with viscoelastic components. This approach was validated by recording the force-displacement and deformation histories from finite element modelling a honeycomb structure. These data compared favourably to experimental quasistatic and dynamic compression testing, validating this novel and convenient route for characterising complex elastomeric materials. Supported by data describing the potential for high build-quality production using an AM process with low barriers to entry, this study should serve to encourage greater exploitation of this emerging manufacturing process for fabricating elastomeric structures within industrial communities.

Keywords

Elastomeric Polymer Characterisation; Hyperelastic; High strain-rate FEA analysis; Cellular Structures; Viscoelastic

1. Introduction

Thermoplastic elastomers (TPEs) are co-polymeric materials that exhibit both thermoplastic and elastomeric properties, with their functional advantages meaning they are used across a broad range of applications. Tooling costs associated with traditional manufacturing methods typically constrains TPE production to high volume components only, limiting opportunities to lever a performance advantage. The emergence of additive manufacturing (AM), with unrivalled design freedom and the economic-viability of one-off production, provides new opportunities to employ TPEs in environments demanding low-volume, high-performance, or both.

Finite element analysis (FEA) simulations are well-established in the design, testing and evaluation of new and novel applications. Emerging techniques including topology optimisation and cellular lattice generation have supplemented this process, guiding designers with an over-riding objective function that prescribes the ultimate mechanical performance [1, 2]. These approaches are now being used in a series of, predominantly metal-based, weight-sensitive applications [3, 4].

The success of optimisation techniques is inherently governed by the accuracy of the material behaviour defined within the simulation. Where the analytical descriptor of a material's behaviour correlates poorly with its physical performance, the simulation will likely deliver an inaccurate solution. TPEs, which exhibit a hyper-elastic (HE) response, can be particularly challenging to characterise due to phenomena such as the Mullin's effect [5], where stress-softening occurs based on the previous level of strain experienced by the material. This results in the material's primary response (i.e. that to the first loading) differing from that of subsequent loading cycles (i.e. the stabilised response). Determining if one, or

both, of these responses are of importance to an application, is key to accurately simulating HE events.

The non-linear HE response of TPE materials means they cannot be characterised by a single data-point. Established constitutive models comprise a series of coefficients associated with strain energy density functions capturing the variation of stress versus strain, with advanced FEA software enabling the end-user to identify the model with the strongest correlation to experimental data. Coefficients describing AM-produced materials typically differ from traditionally manufactured equivalents [6, 7]. Whilst characterisation of AM metallic structures have now been reported [8, 9], no studies quantify the rate-dependant behaviour of HE AM material properties when simulating dynamic events. The technical demands of such characterisation, with laboratories rarely having the requisite facilities including a stand-alone equi-biaxial testing apparatus [10], risks constraining the development and uptake of new TPE AM filaments and powders.

This study describes a novel experimental approach to characterise TPE materials for applications experiencing strain-rates in excess of quasistatic conditions (referred to as dynamic strain-rate applications), using solely a commonplace uniaxial testing machine. Primary, stabilised and rate-dependant responses were captured and then fitted with an appropriate HE/viscoelastic material model. Computational analysis of an exemplar TPE AM structure within a dynamic strain-rate environment demonstrates both the validity of this characterisation process, and the potential to enable high-performance designs.

2. Materials and Methods

Uniaxial, equi-biaxial, and planar tension data was collected to define the HE behaviour; for both primary and stabilised responses. Rate-dependant behaviour was defined by stress relaxation data. For uniaxial, equi-biaxial and planar tests, strain in the gauge area was measured using non-contact video-extensometry (iMetrum CAM028, UK). All stresses and strains are reported as nominal (i.e. engineering) data.

2.1. Materials

Table 1. Printing parameters used for this study

Nozzle Diameter	0.4 mm	Extrusion Multiplier	1.4
Print speed	2000mm/min	Layer Height	100
Bed Temperature	40C	Active cooling	Yes
Extruder Temperature	210	Infill extrusion width	125%

SOLIDWORKS (Dassault Systems, France) was used to design coupons for each test method that were manufactured in NinjaFlex (NinjaTek, US), a readily available TPE filament selected as an exemplar AM material. A fused filament fabrication printer was used (2017 Flashforge Creator Pro printer), retrofitted with high-specification extrusion control (Diabase Engineering, USA) and using processing parameters tuned to achieve a high extrusion density. Simplify3D (Simplify3D, US) was used to alter print settings and slice the .STL files for printing. The common rectilinear pattern was adopted for in-filling the parts and X-ray microscopy (XRM)/microcomputed tomography (µCT) was used to confirm successful fusing of the infill extrudate. Infill was set to 100% and the extrusion settings tuned to ensure fusing of the extrudate, allowing confidence that the infill pattern would have minimal effect on

experimental results. A honeycomb was also designed and manufactured for use as a case study to demonstrate the validity of this novel characterisation methodology, with part quality assessed via µCT. Print orientation is shown in Figure 1.

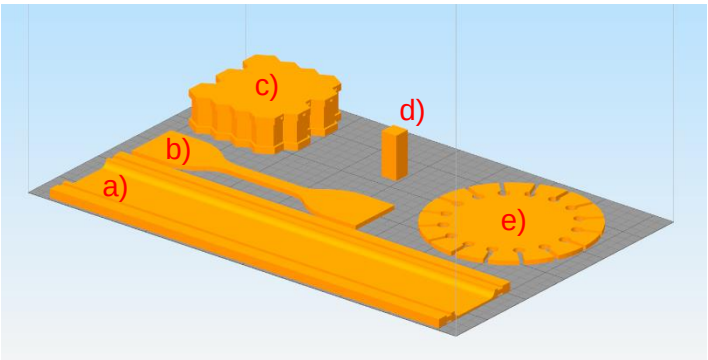

Figure 1. Test part build orientations. a) Planar, b) Uniaxial, c) Honeycomb geometry, d) Cuboid for µCT Scanning, e) Equi-biaxial

2.2. Methods

A preliminary simulation was undertaken to establish the minimum/maximum strains experienced during the loading of the honeycomb structure. This allowed identification of the appropriate cycled strain during mechanical testing, used to describe the stabilised response of the TPE material. A linear elastic model [11] was applied to the honeycomb structure, which was compressed within ABAQUS to densification. The recorded strain was approximately +/- 0.3 throughout the simulated densification of the honeycomb (to ~60% of its original height). This guided the adoption of an upper strain threshold of 0.4 for mechanical testing.

During the preliminary simulation, a mesh sensitivity study was undertaken. Varying the element size from one-quarter, to twice, the wall thickness, achieved near-identical force-displacement curves, and predicted energies also showed little deviance when altering mesh

size. This lack of deviance is consistent with other literature on dynamic compression of cellular structures [12].

Five samples were manufactured for each test setup described in section 2.2.1.

2.2.1. Mechanical Testing

Uniaxial (Tension) Testing

Testing was performed using an electromechanical uniaxial testing machine (Zwick Z50, Germany), following ISO 37 [13] with a reduced crosshead speed (100mm/min), to minimise strain rate sensitivity. Test coupons were designed and fabricated as per tensile testing specimen type 1 [13]. Investigation was performed over cyclical loading to 0.4 strain.

Equi-Biaxial (Tension) Testing

An equi-biaxial test apparatus was designed and built in-house, to enable multi-axial data generation from a single uniaxial testing machine. Novel test coupons were designed and manufactured, including 16 clamping tabs that enabled uniform application of a multi-axial load, generating equi-biaxial strain in the coupon centre (Figure 2 a & b). These test specimens have been shown to be appropriate for equi-biaxial testing [10], with FE analysis showing little influence of geometry on the state of stress in the central gauge section. Machine parameters and cycled strain were consistent with the uniaxial setup.

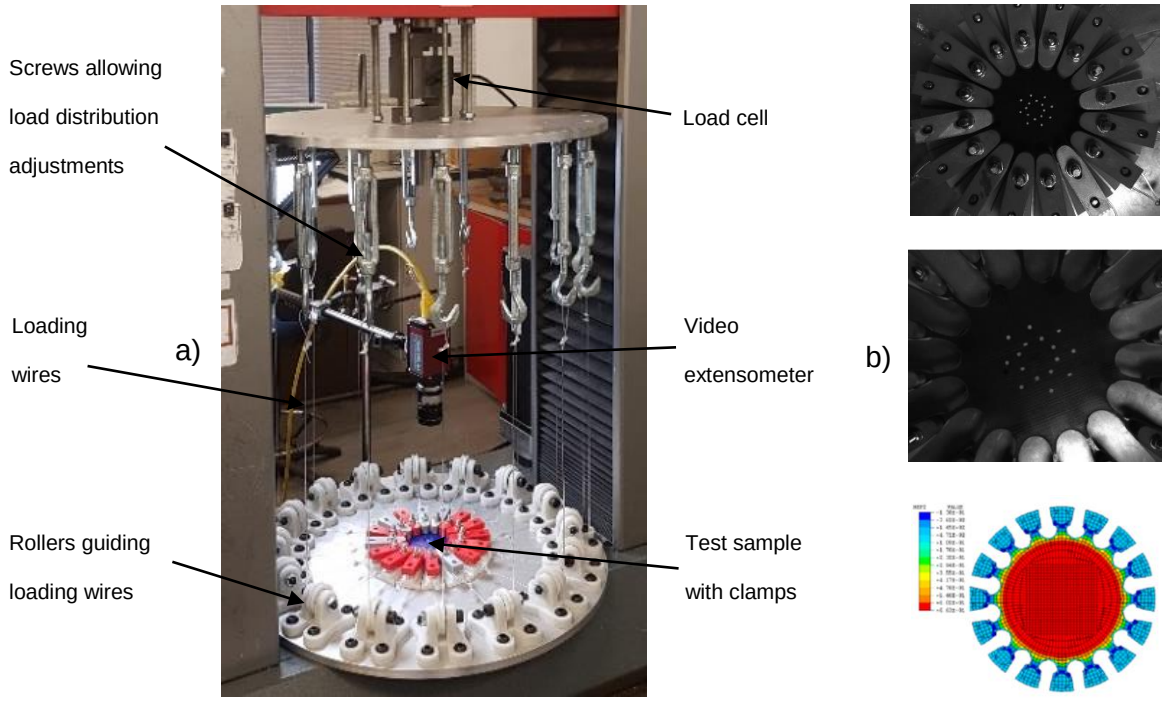

161 *Figure 2: a) Equi-biaxial test rig, b) Stretching of Equi-biaxial sample in this study, and FEA*
162 *validation of sample performed by Day, J. (reproduced from [10])*

163

164 *Planar (Tension) Testing*

165 Shear data is valuable when modelling hyperelastic materials, which is derived from planar
166 tension testing [14, 15]. Novel planar coupons were designed to include ridges, which
167 improved gripping and ensured load distribution into the test gauge area (Figure 3 a & b).
168 Machine parameters and cycled strain were again consistent with the uniaxial setup.

169

170

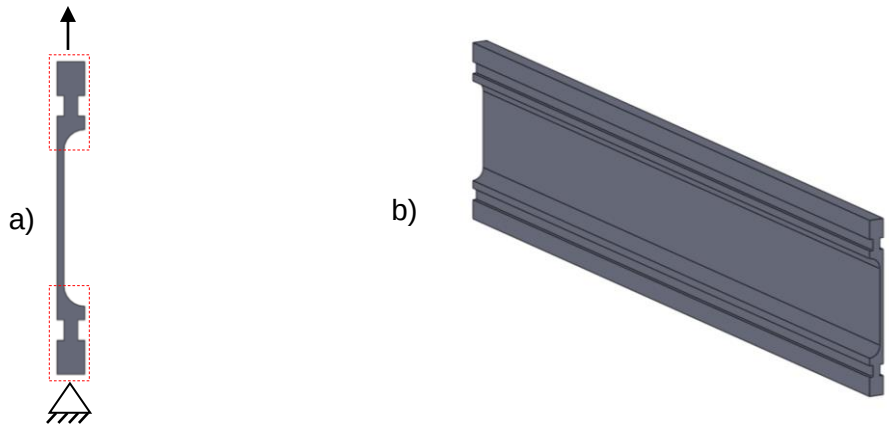

Figure 3: a) Side profile highlighting ridges/added geometry on planar sample, b) 3D visualisation of planar sample

Stress Relaxation Testing

The uniaxial test geometry was used to measure stress relaxation, performed at the maximum available cross-head speed (600mm/min), to a strain of 0.4 and followed by a 100s relaxation period. Stress relaxation experiments cannot achieve an instantaneous step input and will always include an initial loading ramp, as well as inertial effects from the test equipment loading. The user must compensate for these effects when analysing the data, by back-calculating to a theoretical instantaneous load point, as has been performed here.

Mechanical Testing of Exemplar TPE AM Honeycomb

A NinjaFlex hexagonal honeycomb was designed and manufactured to validate the above characterisation process and to demonstrate the potential of AM TPEs to produce structures for high performance applications. The honeycomb structure consisted of a 4x5 unit cell, with each cell having a side length of 5.8mm, 10mm height and 0.4mm wall thickness. Two 3mm thick solid sections were designed onto the upper and lower surfaces of the honeycomb, to achieve well-defined boundary conditions. Exhaust channels (1mm

diameter) were designed in to the lower solid section, enabling release of air trapped within the honeycomb cavities during compression and impact testing.

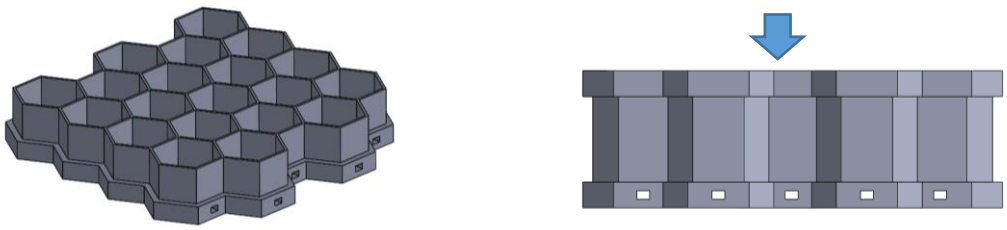

Figure 4. a) sectioned view of the honeycomb part, b) indication of load direction on part

The honeycomb structure was cyclically compressed to densification (~60% of its original height) at 100mm/min (i.e. quasistatically). Industrial-strength adhesive tape (Tesa 64621) was used to adhere the solid sections to the compression platens, ensuring consistent boundary conditions. Dynamic testing was then performed to evaluate the relative performance of the TPE AM honeycomb in a dynamic strain rate environment. A guided drop tower (Instron 9250HV, US) was used to strike the honeycomb test geometry with a 3.53kg impactor at 1.4 m/s. This velocity ensured the honeycomb compressed to >60% of its overall height. An in-line accelerometer (Kistler 8715A, Switzerland) was used to record the acceleration-time pulse. Boundary conditions were defined by: the lower solid section of the honeycomb geometry being adhered to the anvil and, the impactor and upper solid section of the honeycomb being covered with sandpaper. The impactor was released from 0.01m, allowing dynamic compression of the honeycomb to 60% of its original height. Acceleration-time pulses were converted using standard formulae into force-displacement and displacement-time data.

Statistical Analysis

Results of each test method are displayed as a mean value, with error bars representing the standard deviation (SD). All testing was performed through 5 cycles/impacts, to account for stress softening behaviour in the material, which decreased markedly after the second cycle and was cycled a further three times to ensure a stabilised response.

2.2.2. Computational Analysis and Validation

ABAQUS 6.14 (Dassault Systems, France) was used first to curve-fit an appropriate material model to the primary and secondary responses (for dynamic simulations the viscoelastic component was added to these material models), before enabling analysis of the primary and stabilised performance of an exemplar honeycomb structure. An appropriate material model was then selected based on the closest correlation with the test data. Explicit Dynamic analysis was used and, in addition to any other boundary conditions/interactions defined in the simulation, a global frictionless contact was defined to prevent self-penetration of the honeycomb. Incompressibility was assumed (i.e. Poisson's ratio = 0.475, as this is the maximum allowable in ABAQUS) and enhanced hourglass control implemented. Hyper-elastic material models were fitted separately to primary and stabilised datasets. Ogden 1st to 6th order, Polynomial 1st and 2nd order and Reduced Polynomial 1st to 6th order models were investigated for each state. The viscoelastic component of the material model was defined using normalised stress relaxation data, fitted by ABAQUS to a Prony series with 0.001 minimum allowable root-mean-square error. A continuum element hex-dominated mesh was proliferated throughout with a seed equal to the measured average wall thickness of the honeycomb (0.45 mm); however, the 3mm thick upper and lower sections of the test

part were partitioned and given a larger (default) edge seed of 0.72 mm, to reduce the computational cost.

Due to the honeycomb walls being the same thickness as the extrusion nozzle, it was expected the manufactured wall thickness would increase. Average wall thickness was measured by µCT and used to update the honeycomb CAD for ABAQUS simulations. This ensured identical geometry of the simulated and mechanically tested parts.

Quasistatic compression was computationally modelled with the honeycomb component sandwiched between two rigid flat plates. The upper plate was tied to the upper solid section of the honeycomb and prescribed a deflection of 0.6mm, over 1s. The lower plate was fixed in space and tied to the lower honeycomb face. Viscoelastic material properties were not included, whilst a mass scaling of 20 considerably reduced simulation time with minimal influence on accuracy. The force-time and displacement-time histories were extracted from a reference node at the centre of the upper rigid plate, enabling direct comparison with mechanical testing results.

For simulated validation of the impact tests, the honeycomb was again sandwiched between two rigid flat plates in ABAQUS. The upper plate was now assigned a 3.53kg point mass and prescribed a pre-impact velocity observed during experimentation. A sliding frictional coefficient of 1 was defined between the upper honeycomb surface and adjacent plate, to represent a sandpaper-sandpaper contact. The lower honeycomb face was tied to the bottom plate, which was fixed in space. The acceleration-time and displacement-time histories were extracted from a reference node at the centre of the upper rigid plate, for comparison with mechanical testing results. Acceleration-time was converted to force-time using Newton's second law of motion.

2.2.3. X-ray Microscopy (XRM)/Microcomputed Tomography Scanning (µCT)

Porosity analysis was performed using a nominal cuboid structure (7.5 x 7.5 x 20 mm) manufactured from NinjaFlex and adopting the established processing parameters was analysed via XRM using a lab-based Zeiss Xradia 520 (Carl Zeiss XRM, Pleasanton, CA, USA) X-ray Microscope, using a CCD detector system with scintillator-coupled visible light optics, and tungsten transmission target. To achieve a higher resolution over the entire part height, the specimen was imaged along its 20 mm length at high resolution, using an overlap-scan and stitching procedure including five individual scans, with 15% overlap between each scan. An X-ray tube voltage of 60 kV and a tube current of 80 µA were used, with an exposure of 1000 ms and a total of 3201 projections. An objective lens giving an optical magnification of 0.4 was selected with binning set to 2, producing an isotropic voxel (3-D pixel) sizes in the range 11.862 µm. The tomograms were reconstructed from 2-D projections using a Zeiss commercial software package (XMReconstructor, Carl Zeiss), a cone-beam reconstruction algorithm based on filtered back-projection. XMReconstructor was also used to produce 2-D grey scale slices for subsequent analysis. The boundary between pore (gas) and material of the smallest pores (< 2 voxel diameter) will be difficult to define, and therefore the segmentation process could introduce inaccuracies for those smaller pores. Therefore, a threshold size of 2 voxels was implemented and data below this size was excluded.

The honeycomb sample was imaged using a lab-based Nikon XT H225 microfocus X-ray microtomography (µCT) system, with a 1.3 Megapixel Varian PaxScan 2520 amorphous silicon flat panel digital X-ray imager, in reflection mode with a molybdenum target. An X-ray tube voltage of 60 kV and a tube current of 130 µA were used, with an exposure of 1000 ms and a total of 3015 projections, with a voxel (3-D pixel) size of 15.05 µm. The tomograms were reconstructed from 2-D projections using a Nikon commercial software package

(CTPro version 3.0, Nikon Metrology), a cone-beam reconstruction algorithm based on filtered back-projection. The commercial software VGStudio Max 2.1.5 was used to view the reconstructed data and produce 2-D grey scale slices in TIFF format. These were imported into Avizo Software (ThermoFisher Scientific, Waltham, MA, USA), where post-processing including reorientation, binarization, and segmentation allowed extraction of pore size and volume. Honeycomb average wall thickness was measured using Vernier callipers, as well as digitally via the µCT data using SOLIDWORKS (Dassault Systems, France) and used to update the equivalent CAD/FEA model used for computational simulation.

3. Results

3.1. Mechanical Testing

The test results showed that the equi-biaxial response generated a higher stress than the planar response, which was greater than the uniaxial response, at any given strain (Figure 6). This trend was consistent when considering both the primary and stabilised response. Stress and strain for uniaxial and planar testing are presented based on the direction of the loading.

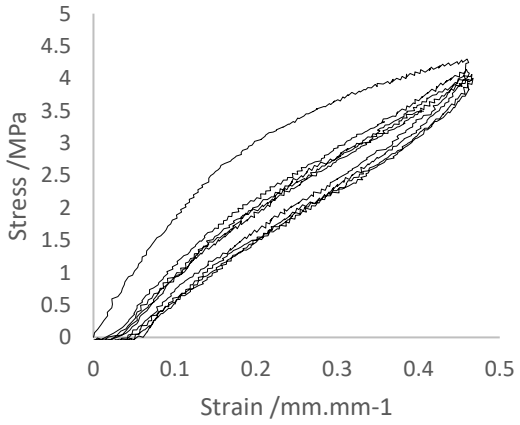

Figure 5. cyclic behaviour of NinjaFlex under uniaxial loading

3.1.1. Primary HE response

All datasets collected demonstrated non-linear behaviour typical of elastomeric materials. Uniaxial testing gave an average initial modulus of 18.2MPa, when considering strains from 0 to 0.1. The average initial planar modulus was 28% greater than uniaxial and the average initial equi-biaxial modulus 66% greater. At a strain of 0.4, uniaxial stress was 4.11 MPa,

planar stress was 4.66 MPa and equi-biaxial stress was 5.13MPa. The full data curves showing the average mechanical test data are displayed in Figure 6.

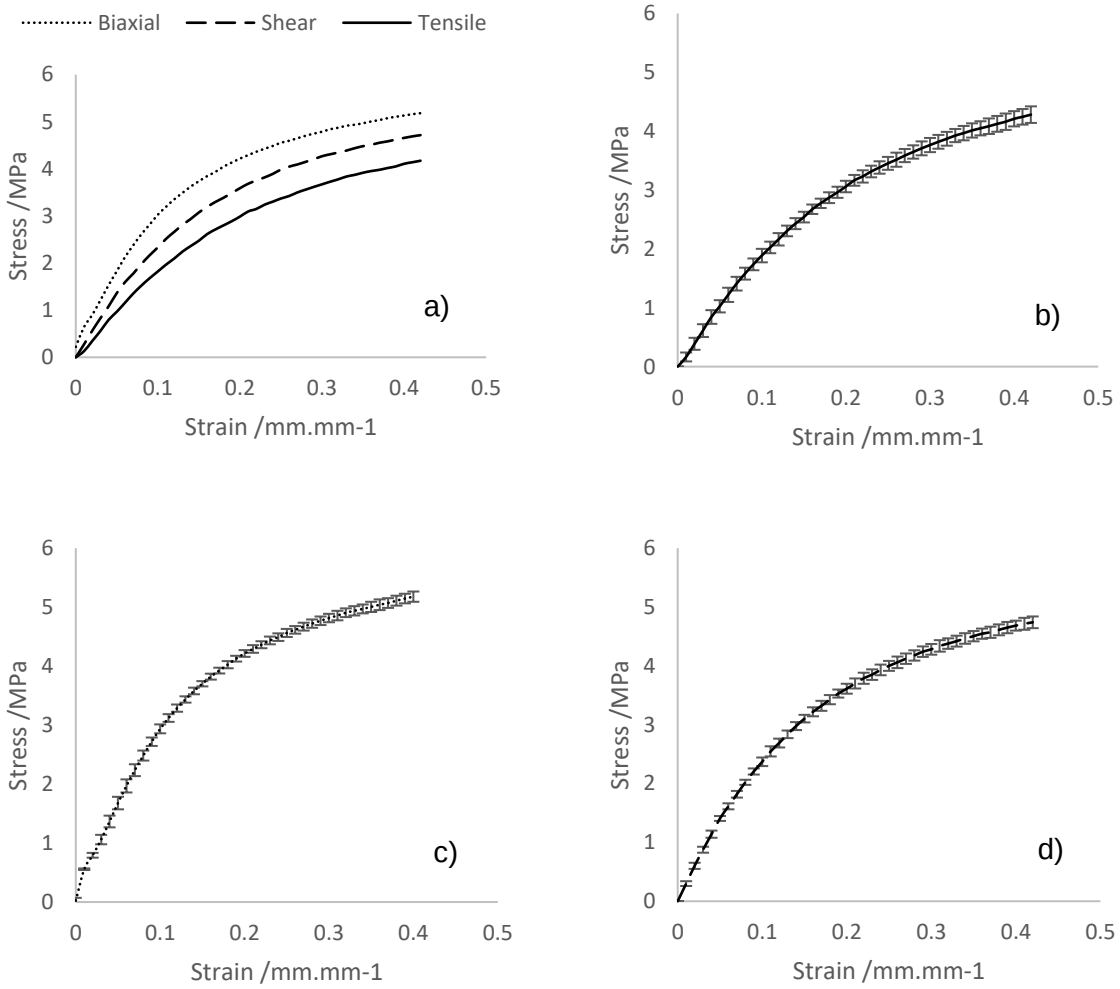

Figure 6 Mechanical testing for average primary response of: a) Combined data sets, b) Uniaxial only, c) Equi-biaxial only, d) Planar only. Error bars = SD

3.1.2. Stabilised HE response

The planar data trend was closer to the uniaxial, than equi-biaxial, response. Uniaxial testing gave an average initial modulus of 12.5MPa, when considering strains from 0 to 0.1.

The average initial planar modulus was 18% higher than uniaxial, and the average initial equi-biaxial modulus was 39% higher. At a strain of 0.4, uniaxial stress was 3.75 MPa, planar stress was 3.97 MPa and equi-biaxial stress was 4.36 MPa. Variance between the 5 test samples for each stress state of the stabilised response was minimal, though larger than the primary response data (Figure 7).

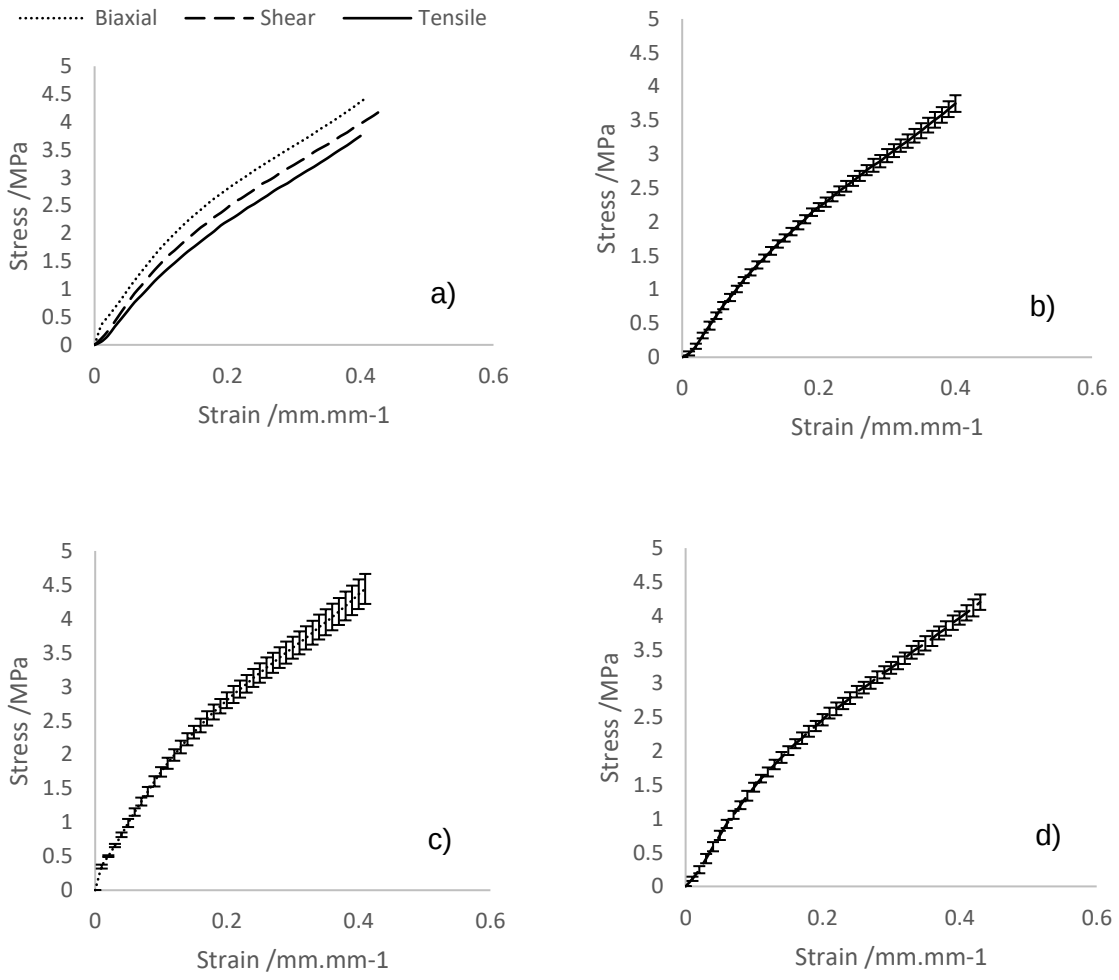

Figure 7 Mechanical testing for the average stabilised response of: a) Combined data sets, b) Uniaxial only, c) Equi-biaxial only, d) Planar only. Error bars = SD

3.2. Curve-fitting

The ABAQUS-based curve fitting procedure for the primary and stabilised responses are presented in Figure 8. The Mooney-Rivlin model provided the most appropriate fit to the primary response, whilst the 2nd order Ogden model provided the best fit for the stabilised response.

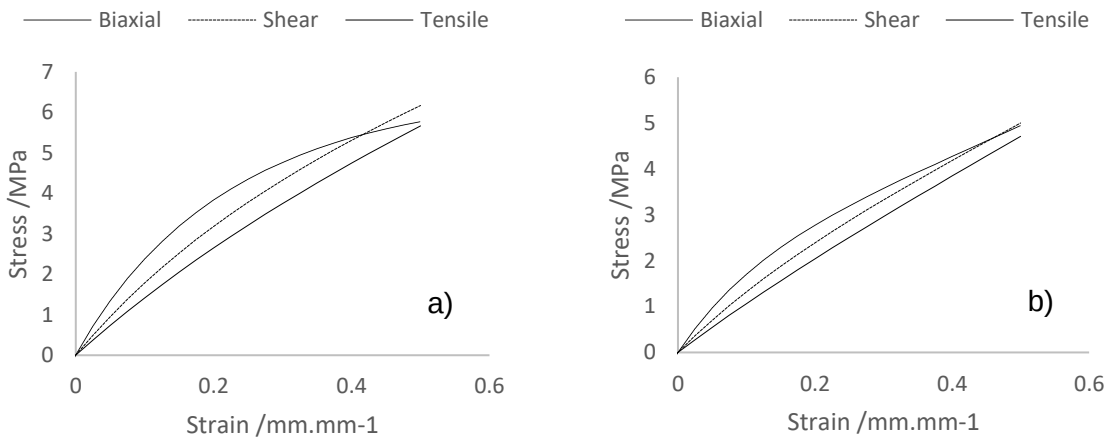

Figure 8 Graphs showing combined fit for: a) Primary response, b) Stabilised response

The coefficients for the primary and stabilised responses material models are presented in Table 2 and Table 3. These models are mathematically stable, both fitting well to experimental extension data and sensibly predicting the compressive behaviour, for the positive and negative strain (+/- 0.3) estimated in the preliminary unit cell investigation (Section 2.2.1). It should be noted that outside of the predicted strain range both models become increasingly inaccurate.

Table 2 Primary response – Mooney-Rivlin material model coefficients

C10 /MPa	*C01 /MPa*
2.93	0.363

Table 3 Stabilised response – 2nd order Ogden material model coefficients

	μ1 /MPa	*α1*
1	12.2	1.87
2	8.41	1.19

Due to the specified low root mean square (RMS) error (0.001), the Prony series were calibrated closely to the experimental data (Figure 9). Examining the experimental data trend enables estimation of a long-term normalised modulus between 0.4 - 0.5. The Prony coefficients that define the curve presented in Figure 9 are quantified in Table 4.

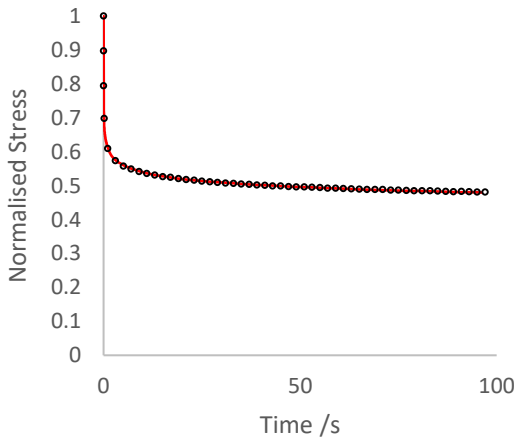

Figure 9 Normalised uniaxial stress relaxation data, with Prony series curve fit

Table 4 Viscoelasticity Prony series

	G /MPa	*K /MPa*	*tau /s*
1	0.196	0.0000	1.27E-03
2	0.129	0.0000	8.30E-02
3	7.67E-02	0.0000	0.894
4	6.03E-02	0.0000	6.51
5	7.10E-02	0.0000	54.6

384 3.3. Honeycomb testing

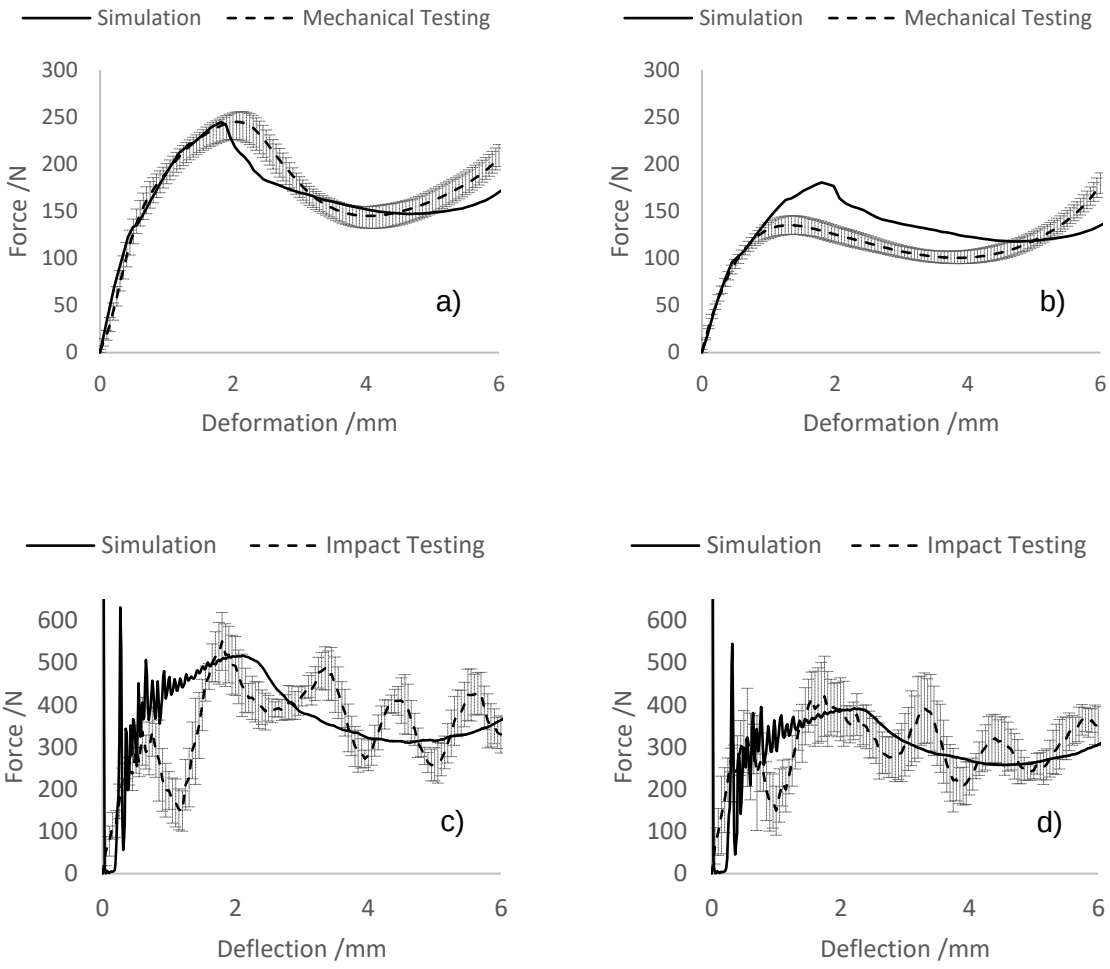

385 *Figure 10 Honeycomb validation, plotting mechanical test data alongside related simulations:*
386 *a) Primary quasistatic, b) Stabilised quasistatic, c) Primary impact, d) Stabilised impact.*
387 *Error bars = SD*

388

389 *Quasistatic Honeycomb Compression*

390

391 The plateau region varies between experimental and simulation results, influencing the
392 energy absorbed by each structure prior to densification (Table 5). For the simulated
393 primary response, agreement exists between the experimental and simulation peak forces
394 and absorbed energy; however, an increase in peak displacement of 11% was observed in

the experimental results. The stabilised energies for the simulated and experimental results were within 10% of one another.

Table 5 Peak quasistatic forces/displacements at commencement of plateau region + energy absorbed by structure prior to densification

	Peak force pre-plateau /N	*Displacement of peak force /mm*	*Energy absorbed by 6mm /J*
Simulation Primary response	245	1.82	1.00
Mean Experimental Primary response	245	2.05	1.04
Simulation Stabilised response	180	1.80	0.77
Mean Experimental Stabilised response	137	1.25	0.69

At 2mm, similar s-shaped and arrow-shaped deformation patterns were observed in experimental testing and simulation (Figure 11). At greater levels of compression (2 – 6mm), the structure begins to fold inside itself with elongated diamond-shaped patterns.

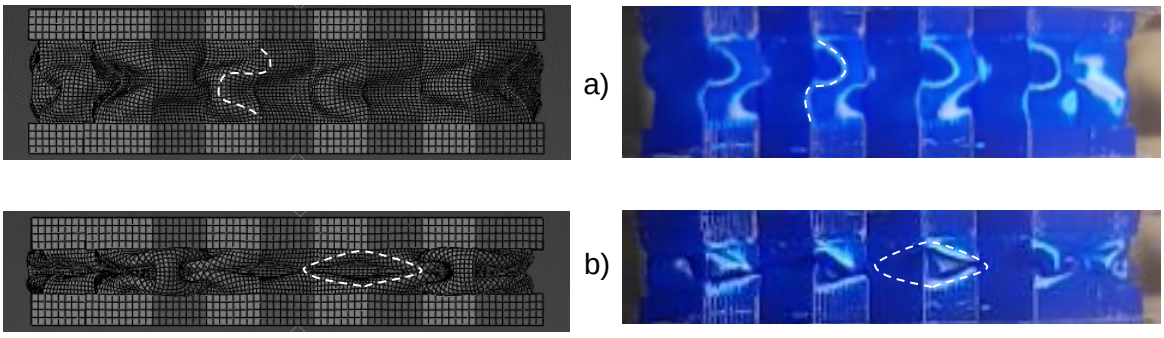

Figure 11 Comparison of simulated and experimental deformation during quasistatic compression: a) 2mm, b) 6mm. Note, simulated images have been mirrored horizontally to highlight deformation patterns.

Data describing the plateau regions is presented in

Table 6. Experimental and simulated peak forces, displacements and energies absorbed were all within 10% of one another for the dynamic primary and stabilised responses, except the stabilised peak displacement, where the mechanical testing was 30% lower.

Table 6 peak forces/displacements at commencement of plateau region + energy absorbed by structure prior to densification dynamic

	Peak force pre-plateau /N	*Displacement of peak force /mm*	*Energy absorbed by 6.5mm /J*
Simulation Primary response	515	1.97	2.21
Mean Experimental Primary response	550	1.80	2.10
Simulation Stabilised response	391	2.20	1.75
Mean Experimental Stabilised response	420	1.75	1.77

Distinct s-shaped deformation was identified both in experimental testing and simulation, at 2mm compression (Figure 12). At 6mm, the experimental testing and simulation demonstrated distinctive arrow-shaped and s-shaped deformation patterns; however, the simulation also had outer walls folding into the centre of the structure, similar to observations during quasistatic compression (Figure 11).

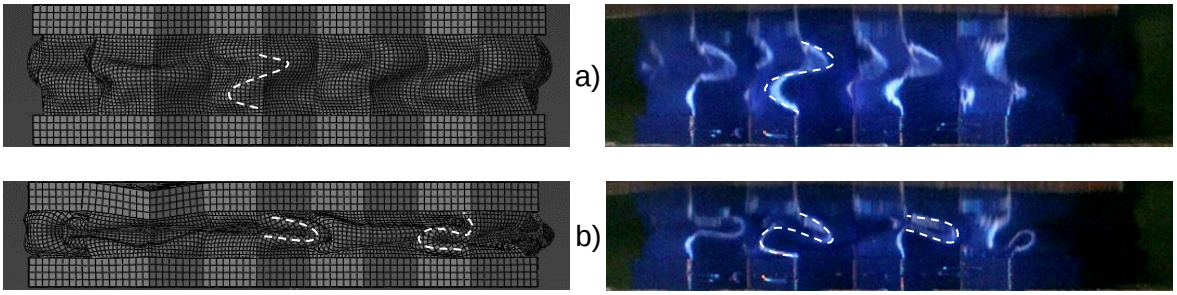

Figure 12 Comparison of simulated and experimental deformation during impact: a) 2mm, b) 6mm. Note, simulated images have been mirrored horizontally to highlight deformation patterns.

3.4. XRM/µCT Analysis

µCT scanning demonstrated that manufactured parts were largely homogenous, meaning successful fusion of the extruded material (Figure 13). Additionally, the outline bounding the internal rectilinear patterning was continuous, with no pores observed throughout its height.

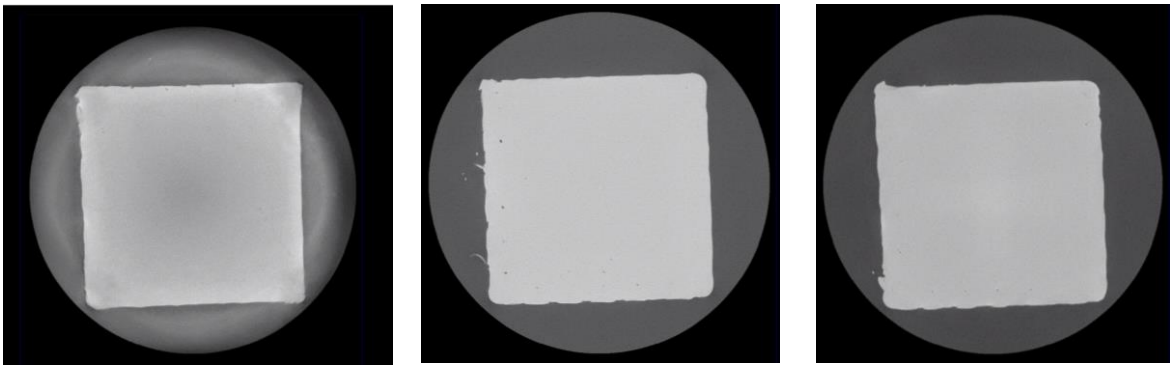

Figure 13 CT scanned cross-sections of cuboid geometry. Left-right: bottom, centre, top

When analysing the pores within the scanned cuboid, those of equivalent diameter ≤2 voxels (equivalent to 23.7 µm) were excluded. This was due to the potential lack of accuracy when detecting pore edges of such small pores. Analysis of the remaining pores suggested the

cuboid was 99.97% dense, with an average pore size of 38 µm and a max pore size of 119 µm. Only ~10% of the pores were 60-119 µm, and these appeared concentrated between the rectilinear fill forming the cuboid centre and the outline forming the perimeter. The distribution of the pores within the cuboid and the pore diameter histogram, are presented in Figure 14. A one-point perspective view down the length of the cuboid illustrates the pore distribution (Figure 14a). The largest pores are located at the boundary of the outline and the infill pattern, in lines running the height of the cuboid.

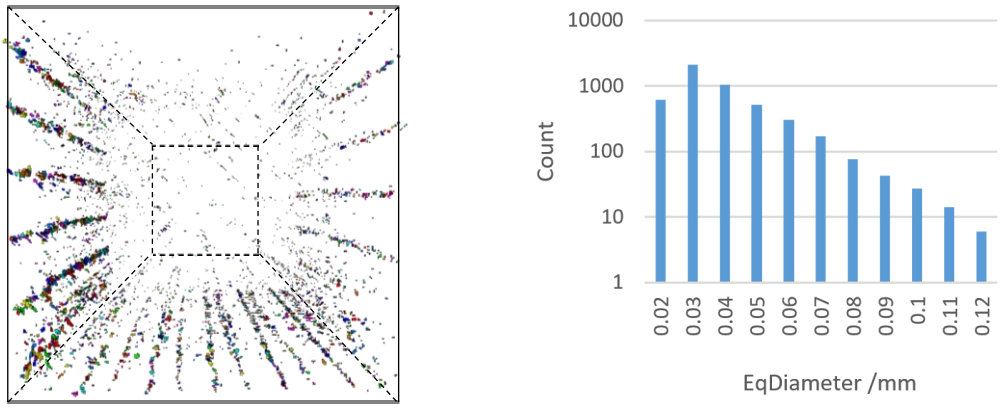

Figure 14 a) 3D image of pores within the cuboid structure, with a bounding outline to show the approximate position of the cuboid exterior, b) histogram showing the effective length of each pore

The µCT scan and supporting vernier measurements of the honeycomb walls gave an average thickness of 0.45mm (versus 0.4mm for the CAD design) with a SD of 0.01 mm. Based on the minimal deviation, the averaged value was used to simulate a part of constant wall thickness within ABAQUS. Some material could be observed drooping as the upper surface 'bridged' over the honeycomb cell wall; however, this appeared minimal and did not affect adhesion between these two features.

4. Discussion

The mechanical performance of TPE AM materials are known to vary with processing parameters, whilst new products regularly enter the market; hence, there is an increasing need to perform full characterisation, though the requisite equi-biaxial facilities remain scarce.

This study has demonstrated success with a novel approach to material characterisation, validated by the comparable trends achieved when experimentally and computationally compressing a honeycomb structure. When applying the material models to a multi-strain rate and state application, a close correlation between predicted and experimental data was observed (Figure 10). The stress-softening characteristic of the Mullin's effect is evident when comparing Figure 6 and Figure 7. Even at a relatively low strain (0.4), the initial stiffness of the primary response is 31% higher than that of the stabilised response, and 15% higher stress at maximum strain. This reinforces the importance of understanding and selecting the correct material response when simulating TPEs in specific applications. This study has also highlighted the need to characterise multiple responses for a single material, with both primary and stabilised responses being required to validate consecutive dynamic compressions of a honeycomb structure (Figure 10).

Good correlation was achieved between the HE material models and experimental data across both the primary ($r^2 = 0.97$) and stabilised ($r^2 = 0.99$) response. Such strong correlation provided a robust platform to investigate dynamic strain-rate applications. The low RMS error requirement placed on the stress relaxation data meant that the viscoelastic portion of the material model closely followed the experimental response. Consequently,

these material models accurately simulate NinjaFlex behaviour in dynamic applications of a similar strain (i.e. +/-0.3).

Applying the material model to the honeycomb structure achieved strong comparability between simulation and experimental data. This strong correlation validates this novel method for TPE characterisation, whilst also demonstrating the potential for use in complex geometries within dynamic environments. The mechanical response (Figure 10) and deformation patterns (Figure 11 and Figure 12) demonstrated excellent prediction of a complex HE buckling event. The quasistatic stabilised experimental and computational investigations exhibited the weakest correlation. This may be caused by the residual strain accumulated during stabilising loading cycles which, in combination with the fixed boundary condition created by the adhesive tape, resulted in a period of tensile loading as the actuator returned to the datum. Whilst this was noted and appropriately adjusted for during data analysis, this additional loading regime could have triggered a unique response within the material, meriting future investigation.

The experimental and simulated honeycombs exhibited discrepancies between their deformation patterns during dynamic loading (Figure 12). Whilst the honeycomb walls appeared to all form s-shaped profiles during experimental testing, a combination of s-shaped and inward folding behaviour was observed in the simulated deformation patterns. This appears to be focussed around the bending of the upper thick section's profile within the simulation, causing inward folding to occur underneath. AM inherently results in wall thickness variation and, whilst the range of wall thickness was minimal and the simulated stress-strain behaviour correlated well with mechanical testing, the lack of this variability could have influenced the deformation pattern observed here. Additionally, the buckling in the structures is a non-trivial event and, therefore, some deviation in deformation patterns was expected between the simulated and experimental behaviour. Structural response can also be influenced by contact behaviour; however, this study investigated pre-densification

behaviour and, when running these simulations with a general frictional contact (as opposed to frictionless), minimal change in stress-strain behaviour was observed.

This study assumed linear viscoelasticity and, whilst the use of non-linear viscoelastic models may help to further fine-tune the prediction of varying strain rate behaviour, this comes at a substantial computational time cost. In the light of this drawback, the close correlation of predicted behaviour presented here serves to justify the assumption of linear viscoelasticity. In the light of mainstream adoption due to low machine costing, fused filament fabrication (FFF) is considered by many to be a rudimentary/entry level technique. The potential of FFF to produce high quality components is, however, demonstrated here, with an excellent cuboid part density of 99.97%. This exceeds previously reported densities achieved via Selective Laser Sintering (SLS) TPE components (~95%) [16] and is comparable to Injection Moulded parts. Accounting for 94% of the cumulative pore volume, the largest voids (70-119µm) are technically challenging to eliminate in FFF builds and existed between the rectilinear fill and bounding outline of the cuboid. During tuning of processing parameters, attempts to reduce these voids included: use of concentric (instead of rectilinear) fill, increasing extrusion multiplier, and increasing overlap between the inner rectilinear fill and bounding outline. These methods introduced their own issues such as the concentric fill generating significant voids in the centre of the part, whilst increasing overlap/extrusion multiplier resulted in distortion of printing parts. It should be noted that the threshold size of 20µm was selected to ensure the pores within the entirety of the cuboid could be captured in a single scan. Whilst this provides a suitable indicator of the porosity of the part (as the pores circa 70-110µm accounted for 94% of the measured pore volume), this has the potential to filter out smaller pores that could have an undetermined influence on material behaviour.

It is known that the layer-by-layer AM build process produces component anisotropy, with this behaviour frequently noted in the literature perpendicular to the layer deposition [17-19].

This behaviour is highly dependent on manufacturing build quality as this logically effects the inter-layer bonding. As complex printed components can be exposed to different strain states, there exists the potential for loadings to be applied parallel and perpendicular to inter-layer bonding even if the overall structure is only under compressive loading. Due to the lack of notable voids, similar deformation patterns/mechanical responses and good correlation between stress-strain behaviour of the honeycomb structure, no further investigation of anisotropy was performed in this study.

As single-track parts (e.g. as per the honeycomb geometry) have no bonding between extrudate in-layer, they can have different mechanical responses than parts with infill patterning (e.g. test parts used to characterise NinjaFlex). Whilst the presence of minimal voids in the recti-linear fill pattern, good correlation between the simulated honeycomb response (using infill patterning characterisation) and mechanical testing (of single extrudate honeycomb print) all indicate this effect was not significant, poor optimisation of printer properties can lead to a disparity in these responses.

5. Conclusions

This study has achieved a greater understanding of the behaviour of TPE AM materials, enabling more effective exploitation of this emerging technology. A novel approach to efficiently and robustly characterise TPE materials has been presented. The importance of considering strain-softening has also been demonstrated, along with the potential to design and analyse AM structures for high performance applications. Highlighted findings include:

- Multi-state strain data to define a material model has been acquired using a standard uni-axial testing machine.
- A material model has been fitted to the TPE test data, including viscoelastic effects. This model is then successfully validated through its application to a case study of a traditional hexagonal honeycomb at varying strain rate.
- The level to which the TPE material was strained had significant effects on subsequent straining of the material, an important consideration when developing material models for applications involving multiple cycling events.
- When dynamically compressed, the viscoelastic properties significantly affect the recorded forces, demonstrating a significant degree of strain-rate dependence. These strain-rate effects carried over to the manufactured parts, resulting in a significant increase in recorded force when dynamically compressed, compared to quasistatic compression.
- FFF has been used to fabricate TPU components of high homogeneity (material density of 99.97%), with expected manufacturing considerations spreading material at the extruder nozzle, resulting in an increased wall thickness.

6. Acknowledgements

M. Robinson was supported by the Knowledge Economy Skills Scholarships 2 (via the Welsh Government's European Social Fund).

The X-ray imaging work was supported by the Advanced Imaging of Materials (AIM) facility (EPSRC grant no. EP/M028267/1), the European Social Fund (ESF) through the European Union's Convergence programme administered by the Welsh Government.

7. Bibliography

1. Huang, X., et al., *Topology optimization of microstructures of cellular materials and composites for macrostructures.* Computational Materials Science, 2013. **67**: p. 397-407.
2. Coelho, P.G., et al., *A hierarchical model for concurrent material and topology optimisation of three-dimensional structures.* Structural and Multidisciplinary Optimization, 2008. **35**(2): p. 107-115.
3. Brackett, D., I. Ashcroft, and R. Hague. *Topology optimization for additive manufacturing*. in *Proceedings of the solid freeform fabrication symposium, Austin, TX*. 2011. S.
4. Leary, M., et al., *Optimal topology for additive manufacture: a method for enabling additive manufacture of support-free optimal structures.* Materials & Design, 2014. **63**: p. 678-690.
5. Mullins, L., *Softening of Rubber by Deformation.* Rubber Chemistry and Technology, 1969. **42**(1): p. 339-362.
6. Mower, T.M. and M.J. Long, *Mechanical behavior of additive manufactured, powder-bed laser-fused materials.* Materials Science and Engineering: A, 2016. **651**: p. 198-213.
7. Gorsse, S., et al., *Additive manufacturing of metals: a brief review of the characteristic microstructures and properties of steels, Ti-6Al-4V and high-entropy alloys.* Science and Technology of Advanced Materials, 2017. **18**(1): p. 584-610.
8. Wadley, H.N.G., N.A. Fleck, and A.G. Evans, *Fabrication and structural performance of periodic cellular metal sandwich structures.* Composites Science and Technology, 2003. **63**(16): p. 2331-2343.
9. Ajdari, A., H. Nayeb-Hashemi, and A. Vaziri, *Dynamic crushing and energy absorption of regular, irregular and functionally graded cellular structures.* International Journal of Solids and Structures, 2011. **48**(3-4): p. 506-516.
10. Day, J. and K. Miller, *Equibiaxial Stretching of Elastomeric Sheets, An Analytical Verification of an Experimental Technique*, in *ABAQUS users' conference*. 2000: Newport, RI. p. 205-220.
11. Ninjatek, *NinjaFlex® 3D Printing Filament*, in *Ninjatek Technical Specifications*, Ninjatek, Editor. 2016, Ninjatek.
12. Abueidda, D.W., et al., *Mechanical properties of 3D printed polymeric cellular materials with triply periodic minimal surface architectures.* Materials & Design, 2017. **122**: p. 255-267.
13. BSI, *BS ISO 37:2017 - Rubber, vulcanized or thermoplastic — Determination of tensile stress-strain properties*. 2017, BSI.
14. Treloar, L.R.G., *The physics of rubber elasticity*. 1975: Oxford University Press, USA.
15. Bergstrom, J.S., *Mechanics of solid polymers: theory and computational modeling*. 2015: William Andrew.
16. Dadbakhsh, S., et al. *Effect of powder size and shape on the SLS processability and mechanical properties of a TPU elastomer*. in *Physics Procedia*. 2016. Elsevier.
17. Frazier, W.E., *Metal Additive Manufacturing: A Review.* Journal of Materials Engineering and Performance, 2014. **23**(6): p. 1917-1928.
18. Soe, S.P., et al., *Mechanical characterisation of Duraform® Flex for FEA hyperelastic material modelling.* Polymer Testing, 2014. **34**: p. 103-112.
19. Ahn, S.-H., et al., *Anisotropic material properties of fused deposition modeling ABS.* Rapid prototyping journal, 2002. **8**(4): p. 248-257.